Available online at www.sciencedirect.com

ScienceDirect

Ceramics International 40 (2014) 2613–2617

CERAMICS INTERNATIONAL

www.elsevier.com/locate/ceramint

Synthesis and characterization of Tb^{3+}/Gd^{3+} dual-doped multifunctional hydroxyapatite nanoparticles

Zhigang Liu*, Qiao Wang, Shaowei Yao, Lirong Yang, Shouwu Yu, Xiaoxin Feng, Fengfeng Li

Hebei Provincial Key Laboratory of Inorganic Nonmetallic Materials; College of Materials Science and Engineering, Hebei United University, Tangshan 063009, Hebei, China

Received 22 August 2013; received in revised form 17 October 2013; accepted 17 October 2013
Available online 26 October 2013

Abstract

Tb^{3+}/Gd^{3+} dual-doped multifunctional hydroxyapatite (Tb^{3+}/Gd^{3+}-HAp) nanoparticles with magnetic and luminescent properties were prepared by the co-precipitation method using $CaCl_2$ and $Na_2HPO_4 \cdot 12H_2O$ as raw materials and CTAB as a template in alkaline conditions. The products were characterized by X-ray diffractometry (XRD), field emission scanning electron microscopy (FESEM), transmission electron microscopy (TEM). Single hexagonal phase Tb^{3+}/Gd^{3+}-HAp nanoparticles were obtained by the co-precipitation method and the products were sphere-like morphology with particle sizes ranging from 40 to 100 nm. Crystallinity degree of the products decreased with the Tb^{3+}/Gd^{3+} substitute increasing. Photoluminescence (PL) and magnetic properties of the products were also investigated. The results show Tb^{3+}/Gd^{3+}-HAp nanoparticles are endowed with strong luminescence at 544 nm and prominent paramagnetic behavior, allowing their potential applications in biological labeling. Gd^{3+} ions sensitize the $^5D_4$-$^7F_5$ transition emission of Tb^{3+} ions in HAp nanoparticles, and the PL emission intensity increases along with increasing concentration of Gd^{3+} ions. Concentration quenching occurs when the Gd^{3+} concentration exceeds 10 mol%. The magnetization level of Tb^{3+}/Gd^{3+}-HAp increased steadily with the doping concentration of Gd^{3+} ions.

Keywords: C. Magnetic; Hydroxyapatite; Lanthanide; Luminescence

1. Introduction

Hydroxyapatite (HAp) is of great value and significance because of its excellent biocompatibility and biological activity [1]. One of the main structural characteristics of HAp is its ability to incorporate a wide variety of substitutions for Ca^{2+}, PO_4^{3-}, and/or OH^- ions in the lattice. The substitution composites of HAp show potential applications in the fields of dental and bone pathologies, bioceramics, luminescence, and catalysis [2–5]. Over past few years, Eu^{3+} or Tb^{3+} doped HAp nanoparticles have attracted extensive attention on the potential applications as luminescent biological labels due to their excellent spectral characteristics and biocompatibility [6–13]. Recently, a novel multifunctional nanostructured system of Eu^{3+}/Gd^{3+} dual-doped HAp was developed that can provide simultaneous image enhancement for magnetic resonance (MR), X-ray and near infrared reflection (NIR) imaging, together with other essential properties such as biocompatibility and target specificity [14,15]. Europium ions, with f–f intra orbital electronic transitions, lead to the photoluminescence of doped nanoparticles, and gadolinium can be used as a contrast agent to provide brighter MR imaging signal.

So far, a number of synthetic routes have been developed for preparing HAp powers, such as, mechanochemistry synthesis [16], the co-precipitation method [17], sol–gel process [18], hydrothermal reaction [19], microemulsion process [13], and microwave irradiation [20]. Among those synthetic routes, the co-precipitation method is a versatile and economic route for the synthesis of homogeneous and pure HAp. Herein, we report a co-precipitation synthesis of Tb^{3+}/Gd^{3+} dual-doped multifunctional hydroxyapatite(Tb^{3+}/Gd^{3+}-HAp) nanoparticles as multifunctional bio-imaging materials with luminescent and magnetic properties. The effects of the Tb^{3+} and Gd^{3+} doping on the structure, luminescent and magnetic properties of HAp nanoparticles are investigated.

2. Material and methods

Multifunctional HAp nanoparticles with magnetic and luminescent properties were prepared by the co-precipitation

*Corresponding author: Tel.: +86 315 2592515.
E-mail addresses: zhgliu@sina.com, zhgliu126@126.com (Z. Liu).

0272-8842/$ - see front matter © 2013 Elsevier Ltd and Techna Group S.r.l. All rights reserved.
http://dx.doi.org/10.1016/j.ceramint.2013.10.070

method using $CaCl_2$ and $Na_2HPO_4 \cdot 12H_2O$ as raw materials and CTAB as a template in alkaline conditions. The terbium and gadolinium sources for the synthesis were terbium oxide (Tb_4O_9; 99.99% pure, Conghua Jianfeng Rare Earth Co. Ltd., Conghua, China) and gadolinium oxide (Gd_2O_3; 99.99% pure, Conghua Jianfeng Rare Earth Co. Ltd., Conghua, China), respectively. All the solvents and other reagents were of analytical grade and were used without any further purification. The experimental water was deionized water. $TbCl_3$ and $GdCl_3$ were prepared by dissolving Tb_4O_9 and Gd_2O_3 in dilute HCl with vigorous stirring, respectively. The superfluous HCl was driven off by heating the solution until the $TbCl_3$ and $GdCl_3$ crystal powders were obtained.

2.1. Synthesis of Tb^{3+}/Gd^{3+}-HAp and pure HAp nanoparticls

In a typical experiment for the synthesis of Tb^{3+}/Gd^{3+}-HAp nanoparticls, a certain amount of $CaCl_2$, $TbCl_3$ and $GdCl_3$ was dissolved in 50 mL of deionized water to form Solution A and the total amount of Ca^{2+}, Tb^{3+} and Gd^{3+} ions was 2.0 mmol. The doping concentration of Tb^{3+} ions was fixed at 2 mol% and that of Gd^{3+} ions was 0 mol%, 5 mol%, 10 mol% and 15 mol% to the total amount of Ca^{2+}, Tb^{3+} and Gd^{3+} ions in mol. $Na_2HPO_4 \cdot 12H_2O$ (1.2 mmol) and CTAB (656.003 mg) were dissolved in 50 mL of deionized water to form Solution B. Then, Solution B was added into Solution A with an addition rate of 2 mL/min under vigorous stirring. Ammonia water was added to adjust pH to 9.5, and the reaction was kept at 30 °C in water bath for 2 h. The products were separated by centrifugation, then washed by deionized water and anhydrous ethanol twice, and finally dried in a vacuum oven at 75 °C. The pure HAp nanoparticls were prepared under the same conditions mentioned above except that terbium and gadolinium chloride were not used.

2.2. Characterization

Phase identification was performed by X-ray diffractometry (XRD, Mode PW3040/60, Philips, Eindhoven, The Netherlands) using nickel filtered CuKa radiation. Morphology of the nanoparticles was inspected using a scanning electron microscope (SEM; S-4800, Hitachi) equipped with an energy-dispersive X-ray spectrum (EDX; XFlash-Detector 4010, Bruker). High resolution imaging of doped HAp was observed by transmission electron microscope (TEM; JEOL-JEM-200CX). The photoluminescence (PL) measurements were performed on a Hitachi F-4500 spectrophotometer equipped with a 150 W xenon lamp as the excitation source at room temperature. The magnetic properties were characterized using a vibrating sample magnetometer (VSM, JDM-13) at room temperature.

3. Results and discussion

3.1. Structure, formation, morphology of pure HA and Tb^{3+}/Gd^{3+}-HAp

Fig. 1 shows XRD patterns of the pure HAp and Tb^{3+}/Gd^{3+}-HAp nanoparticles prepared with the same conditions. It is obvious that all the XRD diffractions of the products can be indexed as a pure hexagonal phase (P63/m space group), agreeing well with the values of the standard data (PDF: 024-0033). Other metal oxide phases related with doped component cannot be detected. Furthermore, it can be found that the relative intensities of the diffractions decrease with the increasing of the Tb^{3+} and Gd^{3+} doping concentrations, indicating the declined crystallinity degree due to the small change in the crystalline structure caused by the mismatch between Ca^{2+} and lanthanide substitution cations. Assuming a homogeneous strain exists across the nanocrystallites, the average crystallite size can be estimated from the full width at half maximum (FWHM) values of diffraction peaks at the angle of $2\theta = 25.889^\circ$ using the Scherrer formula. The results are summarized in Table 1.

SEM and TEM micrographs of as-prepared HAp nanoparticles are shown in Fig. 2. As observed in SEM images (Fig. 2a and b), the undoped HAP and Tb^{3+}/Gd^{3+}-HAp powders were sphere-like morphology, about 40–100 nm in diameter with a little agglomerations. The incorporation of Tb^{3+} and Gd^{3+} ions exerted little influence on the morphology and size of HAp nanoparticles. HRTEM image (Fig. 2c) showed that the 40–100 nm particles in SEM image (Fig. 2b) were agglomerated with about 20 nm similar spherical particles, which is consistent with the average crystallite size (20.3 nm) obtained via broadening analysis (Table 1). In addition, the HRTEM image also provided further insight into the structure of the products. The lattice fringes were observed and the distances (0.347 nm) between the adjacent lattice fringes agreed well with the d_{002} spacing of the literature value (0.344 nm) (PDF:

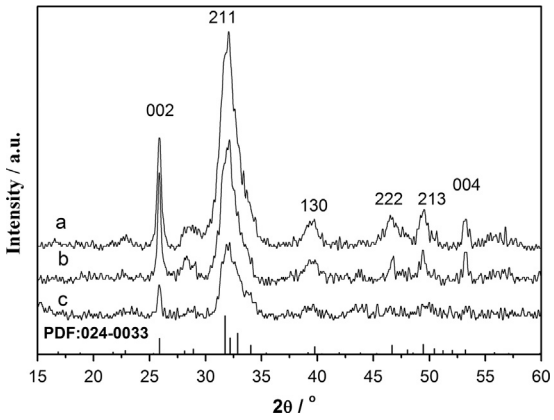

Fig. 1. XRD patterns of the pure HAp and Tb^{3+}/Gd^{3+}-HAp prepared by co-precipitation method at 30 °C, a-HAp; b-2 mol%Tb^{3+}/10 mol% Gd^{3+}-HAp; c-2 mol% Tb^{3+}/15 mol% Gd^{3+}-HAp.

Table 1
Crystallite Sizes of pure HAp and Tb^{3+}/Gd^{3+}-HAp, as Assayed from the Scherrer Equation.

Sample	Doping concentration of Tb^{3+} ions (mol%)	Doping concentration of Gd^{3+} ions (mol%)	Average size of HAp (nm)
1	0	0	23.7
2	2	10	20.3
3	2	15	19.8

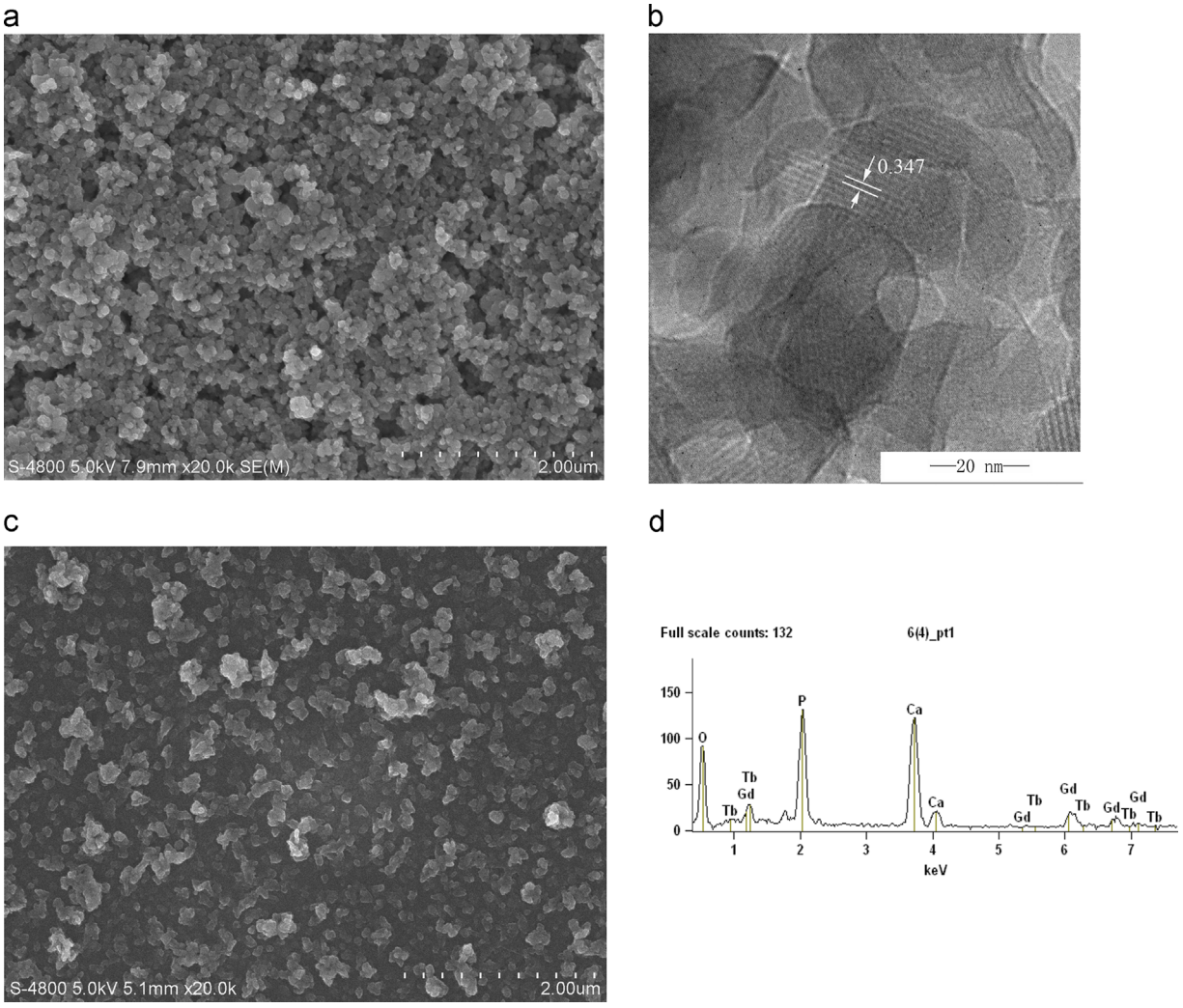

Fig. 2. SEM and HRTEM images of as-prepared HAp nanoparticles: a-SEM images of pure HAp; b- SEM images, c-HRTEM images and d-EDX spectrum of Tb^{3+}/Gd^{3+}-HAp (2mol% Tb^{3+}, 10 mol% Gb^{3+}).

024-0033). The EDX spectrum (Fig. 2d) confirmed the presence of Ca, P, Gd and Tb elements in the Tb^{3+}/Gd^{3+}-HAp nanoparticles. The mole ratio of Gd^{3+} ions to total amount of Ca^{2+}, Tb^{3+} and Gd^{3+} ions was 11.6 mol%. This was calculated according to EDX spectra, which was consistent with the assigned 10 mol% Gd^{3+} doping concentration.

3.2. Effect of Gd^{3+} ion doping concentration on PL properties of Tb^{3+}/Gd^{3+}-HAp

Excitation and emission spectra of as-synthesized Ln^{3+} (Tb^{3+} and Gd^{3+}) doped HAp nanoparticles are shown in Fig. 3. In the excitation spectrum monitored by the Tb^{3+} $^5D_4$-$^7F_5$ transition at 545 nm (Fig. 3a), the broad band with a maximum at 228 nm can be assigned to charge-transfer transitions within the PO_4^{3-} groups [9]. Narrow excitation peaks from Gd^{3+} and Tb^{3+} f→f transitions can be detected at about 311 nm, 352 nm and 369 nm. All the excitation peaks were strengthened due to the incorporation of Gd^{3+} ions, indicating that Gd^{3+} ions sensitized $^5D_4$-$^7F_5$ transition emission of Tb^{3+} ions. In order to investigate the effect of the Gd^{3+} dopant concentration on the PL, the concentrations of Tb^{3+} ions were fixed at 2 mol% and those of Gd^{3+} ions were varied. The excitation wavelength of 228 nm was chosen according to the excitation spectrum. The emission spectra (Fig. 3b) showed that the Gd^{3+} dopants had little effect on the wavelength of emission peaks, but the PL intensity changed considerably by varying Gd^{3+} concentrations. Four emission peaks at about 490 nm, 545 nm, 590 nm and 625 nm appeared. As is known, the most intense peak at 545 nm corresponds to $^5D_4$-$^7F_5$ transition, while the peaks at 490 nm, 590 nm and 625 nm correspond respectively to $^5D_4$-$^7F_6$, $^5D_4$-$^7F_4$, and $^5D_4$-$^7F_3$ transitions. The PL emission intensity increased with increasing concentration of Gd^{3+} ions. The highest PL emission intensity was observed at 10 mol% Gd^{3+} doping, and then decreased remarkably when the Gd^{3+} concentration exceeded the doping amount owing to the concentration quench. The $^5D_4 \rightarrow {}^7F_6$ transition (at 490 nm) is known to be worked by the electric–dipole mechanism, while the $^5D_4 \rightarrow {}^7F_5$ transition (at 544 nm) by the magnetic–dipole mechanism. The peak height ratio F5/F6 is defined as the emission intensity from the $^5D_4 \rightarrow {}^7F_5$ transition divided by that from the $^5D_4 \rightarrow {}^7F_6$ transition. The F5/F6 ratio reveals only slightly

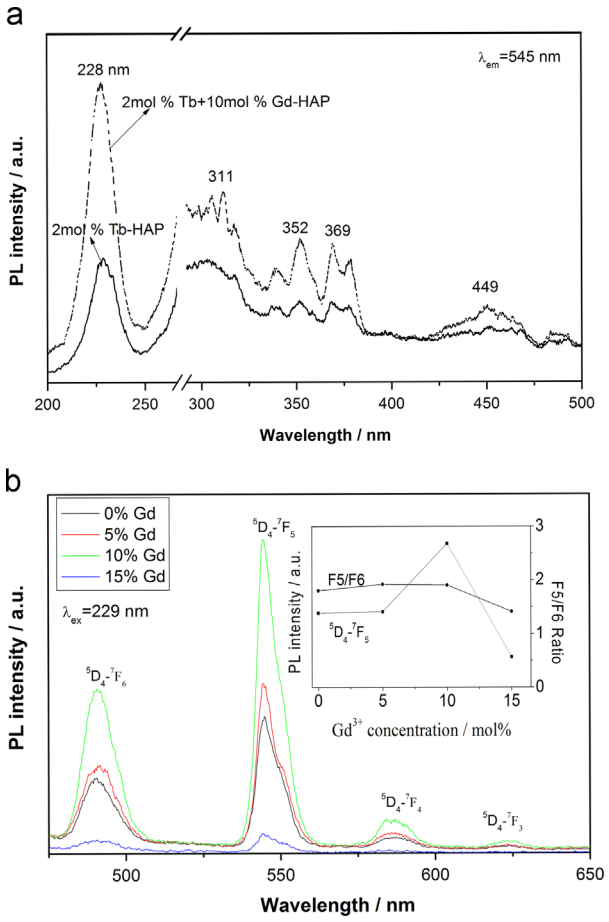

Fig. 3. Excitation and emission spectra of as synthesized Ln^{3+} (Tb^{3+} and Gd^{3+}) doped HAp nanoparticles; a- excitation spectra of Tb^{3+}-HAp and Tb^{3+}/ Gd^{3+}-HAp, and the break is to hide the half frequency peaks, b-emission spectra of Tb^{3+}/ Gd^{3+} doped HAp (Tb^{3+}: 2mol%, and Gd^{3+}: 0, 5 mol%, 10 mol%, and 15 mol%), and inset: variation of emission intensity from the $^5D_4 \rightarrow {}^7F_5$ transition and F5/F6 ratio with Gd^{3+} ions doping concentrations.

variations with increasing Gd^{3+} content, because the electric–dipole transition of Tb^{3+} ions is less affected by the variation of the crystal structure and chemical surroundings.

3.3. Effect of Gd^{3+} ions doping concentration on magnetization of Tb^{3+}/Gd^{3+}-HAp

Fig. 4 shows the room temperature magnetization curves of Tb^{3+}/Gd^{3+}-HAp with different doping amount of Gd^{3+} ions. Obviously, the doped HAp exhibited a paramagnetic behavior. Without Gd^{3+} ions, Tb^{3+}-HAp nanoparticles showed a very low magnetization level. Furthermore, the magnetization level of Tb^{3+}/Gd^{3+}-HAp increased steadily with the doping concentration of Gd^{3+} ions, confirming its predominant role in making the doped HAp magnetically functional. Due to the isotropic electronic ground state $^8S_{7/2}$ and half-filled f-orbit with seven electrons, Gd^{3+} ions possess a high magnetic moment, leading to obvious effects on both longitudinal and transverse proton relaxation of Gd^{3+} ions even at low applied magnetic fields [21]. Tb^{3+}/Gd^{3+}-HAp nanoparticles have a

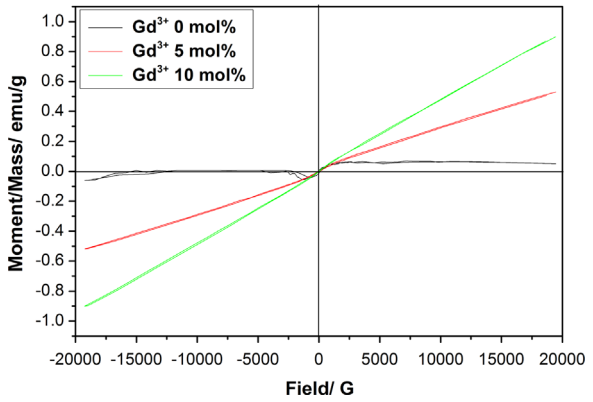

Fig. 4. Room temperature magnetization curves of Tb^{3+}/Gd^{3+}-HAp (Tb^{3+}: 2 mol%, and Gd^{3+}: 0, 5 mol%, 10 mol%).

potential as MR imaging contrast agents because of their positive signal enhancement ability.

4. Conclusions

Tb^{3+}/Gd^{3+}-HAp nanoparticles with magnetic and luminescent properties were prepared by a co-precipitation method. The products are sphere-like morphology with particle sizes ranging from 40 to 100 nm. Tb^{3+}/Gd^{3+}-HAp nanoparticles are endowed with both good luminescence and paramagnetic properties and demonstrate their potential applications in biological labeling. Gd^{3+} ions play a predominant role in sensitizing PL emission of Tb^{3+} ions and enhancing the magnetization level of the Tb^{3+}/Gd^{3+}-HAp nanoparticles.

Acknowledgments

This work was financially supported by the Natural Science Foundation of Hebei Province China (E2011209005), the Education Department of Hebei Province Natural Science Project (2010203) and University Student Innovation Program of Hebei United University.

References

[1] S.I. Stupp, P.V. Braun, Molecular manipulation of microstructures: biomaterials, ceramics, and semiconductors, Science 277 (1997) 1242–1248.
[2] E. Boanini, P. Torricelli, M. Gazzano, R. Giardinob, A. Bigi, Alendronate hydroxyapatite nanocomposites and their interaction with osteoclasts and osteoblast-like cells, Biomaterials 29 (2008) 790–796.
[3] X. Chen, T. Wu, Q. Wang, J.W. Shen, Shield effect of silicate on adsorption of proteins onto silicon-doped hydroxyapatite (100) surface, Biomaterials 29 (2008) 2423–2432.
[4] J.K. Liu, Q.S. Wu, Y.P. Ding, Self-assembled synthesis and fluorescent modification of hydroxylapatite nanoribbons spheres, Eur. J. Inorg. Chem. 20 (2005) 4145–4149.
[5] E. Landi, S. Sprio, M. Sandri, G. Celotti, A Tampieri, Development of Sr and CO_3 co-substituted hydroxyapatites for biomedical applications, Acta Biomater. 3 (2008) 656–663.
[6] A. Doat, F. Pellé, N. Gardant, A. Lebugle, Synthesis of luminescent bioapatite nanoparticles for utilization as a biological probe, J. Solid State Chem. 177 (2004) 1179–1187.

[7] A. Doat, M. Fanjul, F. Pellé, E. Hollande, A. Lebugle, Europium-doped bioapatite: a new photostable biological probe, internalizable by human cells, Biomaterials 24 (2003) 3365–3371.
[8] L. Li, Y. Liu, J. Tao., M. Zhang, H. Pan, X. Xu, R. Tang, Surface modification of hydroxyapatite nanocrystallite by a small amount of terbium provides a biocompatible fluorescent probe, J. Phys. Chem. C 112 (2008) 12219–12224.
[9] C. Yang, P. Yang, W. Wang, J. Wang, M. Zhang, J. Lin, Solvothermal synthesis and characterization of Ln (Eu^{3+}, Tb^{3+}) doped hydroxyapatite, J. Colloid Interf. Sci. 328 (2008) 203–210.
[10] A. Lebugle, F. Pellé, C. Charvillat, I. Rousselot, J.Y. Chane-Ching, Colloidal and monocrystalline Ln(3+) doped apatite calcium phosphate as biocompatible fluorescent probes, Chem. Commun. 6 (2006) 606–608.
[11] O.A. Graeve, R. Kanakala, A. Madadi, B.C. Williams, K.C. Glass, Luminescence variations in hydroxyapatites doped with Eu^{2+} and Eu^{3+} ions, Biomaterials 31 (2010) 4259–4267.
[12] C.S. Ciobanu, SL Iconaru, F. Massuyeau, LV Constantin, A. Costescu, D. Predoi, Synthesis, structure, and luminescent properties of europium-doped hydroxyapatite nanocrystalline powders, J. Nanomater. (2012) (Article ID 942801, 9 pages, http:dx.doi.org/10.1155/2012/942801).
[13] Y. Sun, H. Yang, D. Tao, Microemulsion process synthesis of lanthanide-doped hydroxyapatite nanoparticles under hydrothermal treatment, Ceram. Int. 37 (2011) 2917–2920.
[14] C. Yang, P. Yang, W. Wang, S. Gai, J. Wang, M. Zhang, J. Lin, Synthesis and characterization of Eu-doped hydroxyapatite through a microwave assisted microemulsion process, Solid State Sci. 11 (2009) 1923–1928.
[15] A. Ashokan, D. Menon, S. Nair, M Koyakutty, A molecular receptor targeted, hydroxyapatite nanocrystal based multi-modal contrast agent, Biomaterials 31 (2010) 2606–2622.
[16] T. Isobe, S. Nakamura, R. Nemoto, M. Senna, Solid-state double nuclear magnetic resonance study of the local structure of Calcium Phosphate nanoparticles synthesized by a wet-mechanochemical reaction, J. Phys. Chem. B. 106 (2002) 5169–5176.
[17] S. Kannan, A.F. Lemos, J.M.F. Ferreira, Synthesis and mechanical performance of biological-like hydroxyapatites, Chem. Mater. 18 (2006) 2181–2816.
[18] A. Bigi, E. Boanini, K. Rubini, Hydroxyapatite gels and nanocrystals prepared through a sol–gel process, J. Solid State Chem. 177 (2004) 3092–3098.
[19] S.N. Inés, V.K. Yury, I.L. Oleg, G. Van Tendeloo, et al., An effective morphology control of Hydroxyapatite crystals via hydrothermal synthesis, Cryst. Growth Des. 9 (2009) 466–474.
[20] P. Parhi, A. Ramanan, A.R. Ray, Synthesis of nano-sized alkaline-earth hydroxyapatites through microwave assisted metathesis route, Mater. Lett. 60 (2006) 218–221.
[21] F. Chen, P. Huang, Y. Zhu, J. Wu, C.-L. Zhang, D.-X. Cui, The photoluminescence, drug delivery and imaging properties of multifunctional Eu^{3+}/Gd^{3+} dual-doped hydroxyapatite nanorods, Biomaterials 32 (2011) 9031–9039.